HYDROLOGICAL PROCESSES
Hydrol. Process. **25**, 2531–2541 (2011)
Published online 21 March 2011 in Wiley Online Library
(wileyonlinelibrary.com) DOI: 10.1002/hyp.8025

Characteristics of land surface heat and water exchange under different soil freeze/thaw conditions over the central Tibetan Plateau

Donglin Guo,[1,3]* Meixue Yang[2] and Huijun Wang[1]

[1] *Nansen-Zhu International Research Center, Institute of Atmospheric Physics, Chinese Academy of Sciences, Beijing 100029, China*
[2] *State Key Laboratory of Cryospheric Sciences, Cold and Arid Regions Environmental and Engineering Research Institute, Chinese Academy of Sciences, Lanzhou 730000, China*
[3] *Graduate University of Chinese Academy of Sciences, Beijing 100049, China*

Abstract:

Freezing and thawing processes at the soil surface play an important role in determining the nature of Tibetan land and atmosphere interactions. In this study, land surface water and heat exchanges under different freezing and thawing conditions over the central Tibetan Plateau were investigated using observations from the Coordinated Enhanced Observing Period/Asia-Australia Monsoon Project on the Tibetan Plateau, and the Simultaneous Heat and Water Model. During the freezing and thawing stages, significant diurnal variation of soil temperature resulted in a diurnal cycle of unfrozen water content at the surface. Radiation and energy components and evapotranspiration averaged over four freeze/thaw stages also changed diurnally. On average, the surface albedo (0·68) during the completely frozen stage was sharply higher than those during the freezing, thawing, and completely thawed stages due to the snow cover. The Bowen ratios were 3·1 and 2·5 in the freezing and thawing stages, respectively, but the ratio was only 0·5 in the completely thawed stage. Latent heat flux displayed distinctly better correlation with unfrozen soil water content during the freezing and thawing stages than during the completely frozen and thawed stages. This implies that the diurnal cycle of unfrozen soil water, resulting from diurnal freeze/thaw cycles at the surface, has a significant impact on latent heat flux. A surface energy imbalance problem was encountered, and the possible sources of error were analysed. Copyright © 2011 John Wiley & Sons, Ltd.

KEY WORDS Tibetan Plateau; soil freeze/thaw process; energy closure budget

Received 27 May 2010; Accepted 20 January 2011

INTRODUCTION

The Tibetan plateau has a significant influence on energy and water cycles on both regional scales, such as the Asian monsoon, and global scales, such as El Niño-Southern Oscillation (Flohn, 1957; Yeh *et al*., 1957; Li and Yanai, 1996; Liu *et al*., 2003). The ground absorbs a large amount of solar radiation and undergoes dramatic changes of surface heat and water fluxes due to topographic characteristics (Ye and Gao, 1979; Yanai *et al*., 1992; Tanaka *et al*., 2003). Sensible heating dominates the early summer, whereas latent heating dominates the mid-summer monsoon (Yanai *et al*., 1992). These fluxes drive the intense monsoon circulation and strongly affect global circulation patterns (Webster, 1987; Tanaka *et al*., 2001). Relatively larger net radiation, accompanied by limited latent heat of evaporation resulting from low surface temperature over the Tibetan Plateau, thus heats the atmosphere (Xu and Haginaya, 2001). The thermal effects of the Plateau affect the free atmosphere in terms of turbulence via the near-ground layer and the atmospheric boundary layer. Therefore, it is vital to estimate the land surface heat and water flux exchanges to understand the mechanisms governing the energy cycle over the Asian monsoon region.

Land surface processes over the Tibetan Plateau are multi-featured and complex. Irregular snow cover with permafrost (approximately $1{\cdot}4 \times 10^6$ km^2) and seasonally frozen soil are extensively present. Seasonally freezing and thawing processes in the surface layers and their spatial distribution result in time-space variations of surface wetness and variations of the surface heat balance. Such variations strongly affect the Tibetan seasonal transition (Yang *et al*., 2003), surface energy flux variations (Tanaka *et al*., 2003), and circulation (Wang *et al*., 2003), thus having profound implications for subsequent monsoon behaviour and even global climate processes (Barnett *et al*., 1989; Vernekar, 1995; Su *et al*., 2006).

Typically, soil freezing and thawing processes are accompanied by frequent phase transitions of soil water, resulting in the absorption and release of latent heat. Oscillations in the thermal soil regime and corresponding freeze/thaw cycles engender concomitant changes in the energy and water exchanges between land surface and atmosphere (Yang *et al*., 2007a). The land surface energy and water exchanges are quite different under frozen or thawed soil conditions (Li *et al*., 2002). In addition, the near-surface experiences diurnal freeze/thaw cycles

* Correspondence to: Donglin Guo, NZC, Institute of Atmospheric Physics, Chinese Academy of Sciences, Beijing 100029, China.
E-mail: guodl@mail.iap.ac.cn

over half the year (Yang *et al.*, 2007a). Therefore, the freeze/thaw processes of the surface layer are important factors in the land-atmosphere interactions.

It is difficult to make conventional *in situ* measurements on the Tibetan Plateau because of its rugged and varied topography. Consequently, the Global Energy and Water Cycle Experiment/Asian Monsoon Experiment on the Tibetan Plateau (GAME-Tibet, 1996–2000) and the Coordinated Enhanced Observing Period/Asia-Australia Monsoon Project on the Tibetan Plateau (CAMP-Tibet, 2001–2005) were conducted by a joint Chinese-Japanese field team. By using the collected data, some studies associated with the surface energy budget and closure as well as seasonal and diurnal variations of surface heat flux components, soil temperature, and soil moisture have been reported (Kim *et al.*, 2000a, 2000b; Gao *et al.*, 2000a, 2000b, 2004; Tsukamoto *et al.*, 2001; Tanaka *et al.*, 2001, 2003; Ma Y, *et al.*, 2004, 2006; Yang *et al.*, 2003, 2007a; Ma and Ma, 2006; Guo et al., 2009a, 2009b; Guo and Yang, 2010; Guo et al., 2011). However, few works have focused on the impact of near-surface diurnal freeze/thaw cycles on energy and water exchanges between the land surface and atmosphere.

The objectives of this work are to investigate the average diurnal variations of radiation fluxes, soil heat flux, soil temperature, and unfrozen soil water in each of the four freeze/thaw stages from observations. Diurnal variations of sensible heat flux, latent heat flux, and evapotranspiration averaged in the four stages were also investigated with simulated data. Additionally, the impact of near-surface diurnal freeze/thaw cycles on surface heat flux was preliminarily evaluated with observed soil temperature and unfrozen soil water as well as simulated sensible and latent heat fluxes. Finally, the surface energy budget was analysed using the closure ratio, which was calculated by the observed net radiation, calculated soil heat flux, and the simulated sensible and latent heat fluxes.

DATA AND METHODS

Field measurement data

Site 'BJ' (31·37 °N, 91·90 °E; 4509 m) is an observational station of the CAMP-Tibet project located in a relatively large open space and covering an area of approximately 30 × 50 km on flat Naqu grassland in a seasonally frozen soil region of the central Tibetan Plateau (Figure 1). Soil is predominantly sandy silt loam with small and scattered pebbles, and vegetation cover consists of short grass with a canopy height less than 0·05 m and a leaf area index (LAI) less than 0·5 during the peak growth stage in late May to mid-September (Gao *et al.*, 2004). Details on the instruments and various data–processing techniques are provided in corresponding documents at the following Web sites: http://data.eol.ucar.edu/codiac/dss/id=76·127 and http://data.eol.ucar.edu/codiac/dss/id=76·128.

General information on observational elements collected at site BJ are shown in Table I. Net radiation was measured at 1·5 m above the ground with CM-21 (Kipp & Zonen), which measured downward short-wave/long-wave and upward short-wave/long-wave radiation separately. The thermal effects owing to sensor

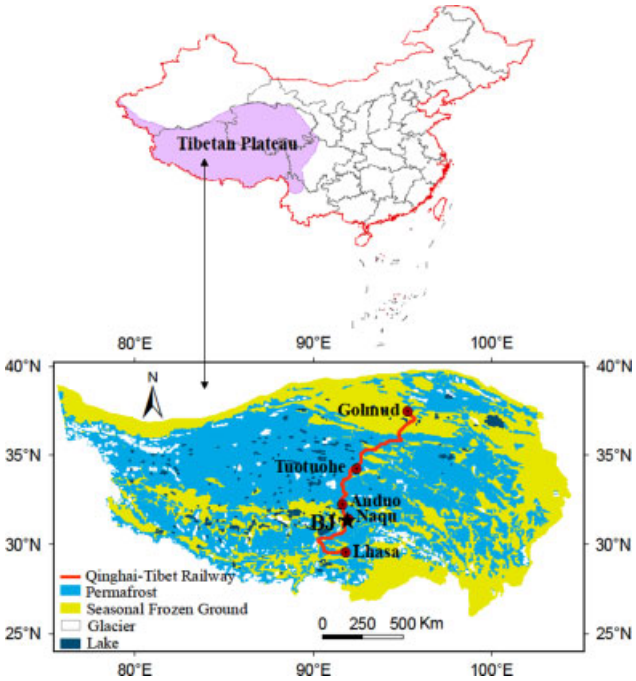

Figure 1. Distribution of frozen ground (after Li and Cheng, 1996) and geographic location of the study sites

Table I. Observational elements at site BJ

Observational elements	Height/m	Instrument type, manufacturer
[a]wind speed/m s^{-1}	10, 5, 1	WS-D32, Komatsu
wind direction/°	10	WS-D32, Komatsu
[a]air temperature/ °C	8·2, 1	Ts-801, Okazaki
[a]specific humidity/%	8·2, 1	HMP-45D, Vaisala
atmospheric pressure/hPa	ground	PTB220C, Vaisala
[a]precipitation/mm	ground	NOAH-II, ETI
[a]radiation flux/W m^{-2}		CM-21, Kipp & Zonen
soil heat flux/(W m^{-2})	−0·1, −0·2	MF-81, EKO
[a]soil temperature/ °C	−0·04, −0·2, −0·4, −0·6, −0·8, −1·0, −1·3, −1·6, −2, −2·5	Pt100, Datamark
[a]unfrozen soil water/m^3 m^{-3}	−0·04, −0·2, −0·6, −1·0, −1·6, −2·1	Trime EZ, Imko

[a] elements were used as forcing data for SHAW model simulation.

temperature were taken into account when calculating long-wave radiation components. The soil heat flux was measured at depths of 0·1 and 0·2 m with MF-81 (EFO). Fluxes of sensible heat and latent heat were measured by an eddy covariance system (KAIJO-DA600, Kaijo; Li-7500, Li-Cor). These instruments were mounted at 3 and 20 m above the ground facing prevailing wind directions, with raw data sampled every 0·1 second (10 Hz). Post-processing of the data was performed for quality control, and various corrections were applied to minimize the measurement errors. More detailed information can be found in the works of Kim *et al*. (2000a), Choi *et al*. (2004), Gao *et al*. (2004), and Ma Y, *et al*. (2004). The eddy covariance data were measured during the periods from 24 November 2002 to 19 December 2002, and from 3 June 2003 to 30 June 2003 and were derived from http://data.eol.ucar.edu/(visited on 1 January 2010). Data flagged B (bad) or D (dubious) were eliminated and can be used to validate the model. Surface soil temperature and unfrozen soil water at different depths were observed during 23 August 2002–23 May 2003 to specifically reveal the surface diurnal freeze/thaw cycles. At the BJ site, twelve platinum temperature probes were installed at depths of 0, 0·005, 0·01, 0·02, 0·03, 0·04, 0·05, 0·06, 0·07, 0·08, 0·09, and 0·2 m. In addition, four time-domain reflectometers were installed horizontally at depths between 0–0·03, 0·03–0·06, 0·06–0·09, and 0·185 m–0·215 m for monitoring unfrozen soil water content. All of the probes were connected with two dataloggers recording at 30-min intervals. The monthly snow depth data at the Naqu meteorological station during 1966–1999, derived from SSM/I (Special Sensor Microware/Imager), were also used in our analysis.

Methods

Four soil freeze/thaw stages were defined without consideration of the effect of salinity on the soil freezing point. These stages are completely thawed (i) where daily minimum soil temperature is $>0\,^{\circ}$C); completely frozen, (ii) where daily maximum soil temperature is $<0\,^{\circ}$C); freezing, (iii) where the soil profile is in the process of freezing); and thawing (iv) where soil profile is in the process of thawing) (Yang *et al*., 2007a; Guo *et al*., 2011). To avoid the potential impact of random weather processes on the movement from one stage to the next, the passage of three consecutive days meeting a chosen category of criteria was used as the indicator of the transition, and the first day of these three days was recorded as the start date of the next freeze/thaw stage. Based on this assumption, four freeze/thaw stages were identified at a depth of 0·02 m: freezing from 3 October to 31 December, completely frozen from 31 December to 25 January, thawing from 25 January to 14 May, and completely thawed from 14 May to 3 October.

Eddy fluxes were calculated by the following equations (Ma *et al*., 2004):

$$H = \rho C_p \overline{w' T'}, \tag{1}$$

$$LE = \rho L \overline{w' q'}, \tag{2}$$

where H, LE, and E refer to sensible heat, latent heat, and evapotranspiration, respectively. ρ,C_p, and L are the density of air (kg m^{-3}), the specific heat of air (J kg^{-1} K^{-1}), and latent heat of vaporisation (J kg^{-1}), respectively. w', T', and q' are the fluctuations of the vertical wind component (m s^{-1}), air temperature (K), and specific humidity (g kg^{-1}), respectively.

The ground soil heat flux (G_0) was calculated using the method described in Yang and Wang (2008), which can be applied to surface energy budget analysis in atmospheric boundary layer experiments (Yang *et al*., 2003). Meanwhile, we added a freeze/thaw term (δ) for the change of unfrozen soil water content. The equation is as follows:

$$G = G(z_{ref}) + \frac{1}{\Delta t}\sum_{z_{ref}}^{z}[\rho_s c_s(z_i, t+\Delta t)T(z_i, t+\Delta t) - \rho_s c_s(z_i, t)T(z_i, t)]\Delta z + \delta, \tag{3}$$

Under $T(z_i, t) > 0\,^{\circ}$C, $\delta = 0$;
Under $T(z_i, t) < 0\,^{\circ}$C, $\delta = \frac{1}{\Delta t}\rho_w c_w[\theta_w(z_i, t+\Delta t) - \theta_w(z_i, t)]\Delta z$,

When adding the freeze/thaw term, we assume that unfrozen water content is not changing significantly due to evaporation and liquid water movement. This could be a fair assumption as long as ice is present ($T(z_i, t) < 0\,^{\circ}$C) in the soil. The soil heat capacity ($\rho_s c_s$) can be calculated by the following formulas (Sellers *et al*., 1996a; Oleson *et al*., 2004):

$$\rho_s c_s = \rho_{dry} c_{dry} + \rho_w c_w \theta_w + \rho_{ice} c_{ice} \theta_{ice}, \tag{4}$$

where θ_w (m^3 m^{-3}) is the unfrozen soil water content, θ_{ice} is the soil ice content from the simulated results (m^3 m^{-3}), $\rho_{dry} c_{dry}$ (J kg^{-1} K^{-1}) is the heat capacity of a dry soil [$\approx (1 - \theta_{sat}) \times 2{\cdot}1 \times 10^6$)], θ_{sat} (m^3 m^{-3}) is the soil porosity, $\rho_w c_w$ (J kg^{-1} K^{-1}) is the heat capacity of liquid water ($\approx 4{\cdot}2 \times 10^6$), and $\rho_{ice} c_{ice}$ (J kg^{-1} K^{-1}) is the heat capacity of ice ($\approx 1{\cdot}9 \times 10^6$).

Net radiation (Rn) was calculated by the following equation:

$$Rn = DS + DL - US - UL, \tag{5}$$

where DS, DL, US, and UL refer to downward short-wave (W m^{-2}), long-wave radiation (W m^{-2}), upward short-wave (W m^{-2}), and long-wave radiation (W m^{-2}), respectively.

Hourly averaged values (p) of any variable R in a certain freeze/thaw stage were calculated by the following equation,

$$p_i = \frac{1}{n}\sum_{j=1}^{n} R_{i+24\times(j-1)} \qquad (i = 1, 2, \ldots, 24). \tag{6}$$

where i refers to the time of day, p_i is hourly averaged value of the variable R at the i^{th} hour in a certain freeze/thaw stage, and n is amount of days for a certain freeze/thaw stage.

Model and parameter setting

The Simultaneous Heat and Water (SHAW) model was developed by Flerchinger and Saxton (1989) and consists of a vertical, one-dimensional profile extending from the vegetation canopy, snow, residue, or soil surface to a specified soil depth. A layered system is established through the plant canopy, snow, residue, and soil, with individual nodes representing each layer. Energy, moisture, and solute fluxes are computed between nodes for each time step. Unique features of the model include the simultaneous solution of heat, water, and solute fluxes as well as detailed provisions for soil freezing and thawing. Heat and water fluxes into the system are defined by diurnal or hourly weather conditions (air temperature, wind speed, humidity, solar radiation, and precipitation) above the upper boundary and soil conditions at the lower boundary. The model not only considers the impact of unfrozen water, ice, and, vapour transfer on the water and heat balances, but also the latent heat flux generated when soil undergoes freezing or thawing. Soil volumetric water content is expressed as a function of matric potential.

The SHAW model requires flexible parameter settings. Water and heat conditions at the lower boundary and hydraulic parameters may either be calculated or prescribed. In this study, hydraulic parameters were automatically calculated by the model according to soil texture. Soil was divided into 12 layers, and the soil texture of each sub-layer was obtained from Luo *et al.* (2008) (Table II). The *in situ* elements marked with letter 'a' in Table I were used as forcing data for model simulations from 1 August 2002 through 31 August 2003. The fraction of surface covered by canopy was 0·45 (Gao *et al*., 2004); the surface roughness was 0·00466 m (Ma Y, *et al*., 2002); the height of the canopy top was 0·05 m (Gao *et al*., 2004); the root depth was 0·3 m (Gao *et al*., 2004); and the characteristic dimension of canopy leaves was 0·01 m (Sellers *et al*., 1996b). Monthly leaf area index of the canopy was obtained from a monthly composite of the NASA MODIS LAI MOD15A2 product with 1 km spatial resolution (available at: ftp://primavera.bu.edu/pub/datasets/, visited on 10 August 2009).

RESULTS AND DISCUSSIONS

Validation of the model

The SHAW model was validated by assessing the level of agreement between the measured and simulated sensible heat flux, latent heat flux, and evapotranspiration. Simulated hourly sensible flux, latent heat flux, and evapotranspiration were compared with direct measurements during the periods 3 June 2003 to 30 June 2003 and 24 November 2002 to 19 December 2002 (Figure 2). The simulated sensible heat flux, latent heat flux, and evapotranspiration are in close agreement with measured results during the 3 June 2003 to 30 June 2003 period. However, the model underestimated the diurnal maximum sensible heat flux on 11 June and 30 June and overestimated the diurnal maximum latent heat flux and evapotranspiration on 4 June and 25 June. Their linear correlation coefficients were 0·87, 0·92, and 0·92 (above 99% confidence level, used throughout) with mean biases of 5 W m^{-2}, 8 W m^{-2}, and 0·01 mm, respectively.

Between 24 November 2002 and 19 December 2002, the simulated sensible heat flux fit closely with measured results, with a linear correlation coefficient of 0·95 and a mean bias of 10 W m^{-2}. The simulated latent heat flux and evapotranspiration also show good agreement with observed results, except that the model underestimated the maximum latent heat flux and evapotranspiration on 27 November and 28 November. Their linear correlation coefficients were 0·76 and 0·73, with mean biases of 2 W m^{-2} and 0 mm, respectively. Thus, the SHAW model can reasonably simulate the sensible heat flux, latent heat flux, and evapotranspiration at the BJ site on the central Tibetan Plateau.

The simulated soil temperature at depths of 0 m and 0·04 m and unfrozen soil water content at depths of 0·04 m were also compared with direct measurements during the 2 December 200 224 December 2002 period

Table II. Input soil temperature, unfrozen soil water, and soil texture

Depth/m	Unfrozen soil water/m^3 m^{-3}		Soil temperature/°C		Soil texture/%		
	start	end	start	end	sand	clay	silt
0.0	0·237	0·22	25·5	16·3	74	22	4
0.04	0·210	0·215	13·9	13·1	74	22	4
0.1	0·183	0·177	14·2	13·4	74	22	4
0.2	0·138	0·139	12	11·6	74	22	4
0.4	0·137	0·123	12·6	11·9	53	36	11
0.6	0·166	0·109	12·7	12	89	7	4
0.8	0·209	0·166	12·5	12	94	5	1
1.0	0·253	0·222	11·6	11·1	94	5	1
1.3	0·260	0·240	10·8	10·5	93	5	2
1.6	0·265	0·252	10·5	10·3	93	5	2
2.0	0·274	0·268	9·4	9·4	93	5	2
2.5	0·285	0·301	8·4	8·4	93	5	2

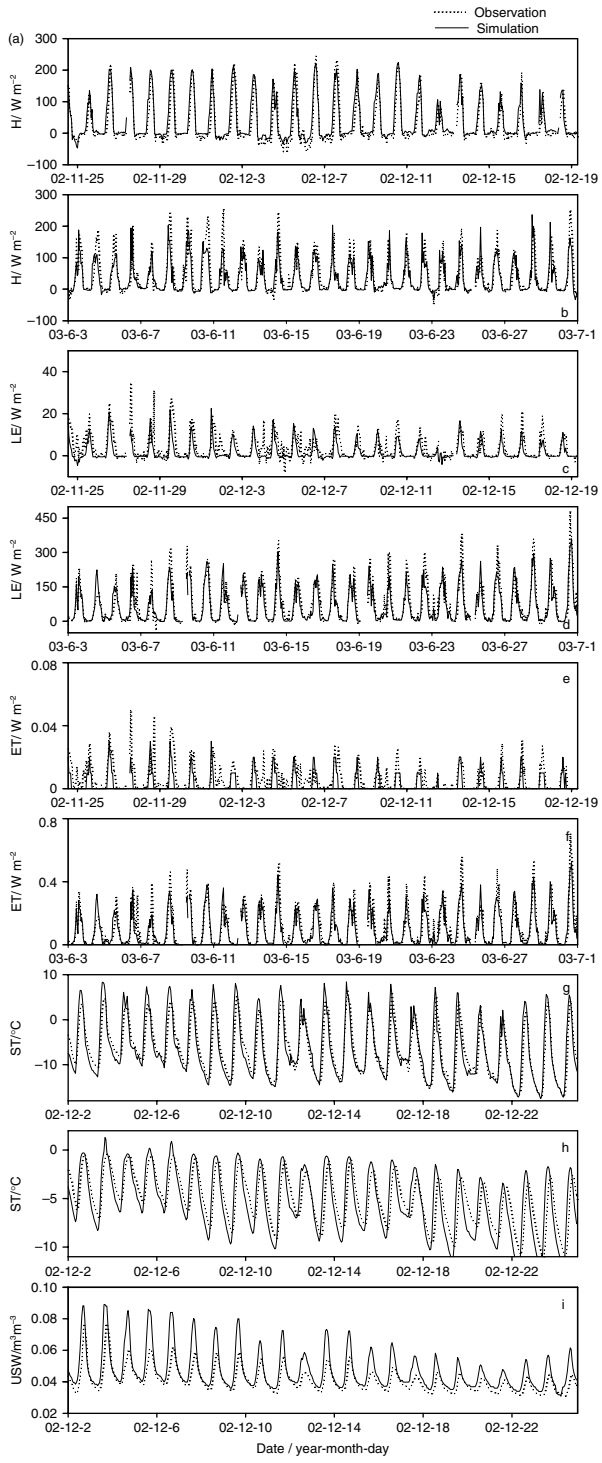

Figure 2. Comparison of simulated and observed hourly net radiation, sensible heat flux (H), a and b, latent heat flux (LE), c and d, evapotranspiration (ET), e and f,), soil temperature (ST) at depths of 0 m, g and 0·04 m, h, and unfrozen soil water (USW) at a depth of 0·04 m, i

(Figure 2). Apparently, the simulated soil temperature fits well with the measured data, although the model overestimated the diurnal maximum soil temperature at a depth of 0 m. Their linear correlation coefficients were 0·94 and 0·89, with mean biases of −0·2 and 0·28 °C for 0 m and 0·04 m depths, respectively. The simulated and observed unfrozen soil water content had a correlation coefficient of 0·91 and mean bias of 0·01 m^3 m^{-3}. The model also overestimated the diurnal maximum unfrozen soil water content. Because soil water freezing depends on soil temperature change, the performance of the model to simulate soil temperature can provide a basic evaluation of the accuracy of the simulated soil ice content used in Equation (4).

Diurnal variation of land surface heat and water fluxes averaged in different freeze/thaw stages

Observed diurnal variation of soil temperature and unfrozen soil water. Diurnal amplitudes of soil temperature and unfrozen water content were lower at deep soil (Figure 3). Diurnal amplitudes of soil temperature and unfrozen water content at 0·02 m depth were distinctly larger than those at 0·04 m for all freeze/thaw stages. The diurnal variation pattern of soil temperature at 0·04 m depth was similar to that at 0·1 m depth for all freeze/thaw stages. In the completely thawed stage, the minimum and maximum values of soil temperature occurred at the following site times (used throughout) and depths: 5 : 00 and 13 : 00 for 0·02 m depth, 6 : 00 and 15 : 00 for 0·04 m depth, 6 : 00 and 14 : 00 for 0·1 m depth, respectively. At the same depth, diurnal patterns of soil temperature were similar in different freeze/thaw stages; however, unfrozen soil water in the completely frozen and completely thawed stages showed relatively weak diurnal signatures compared to the significant diurnal cycles in the freezing and thawing stages.

Diurnal ranges of soil temperature at 0·02 m depth were large and reached 23 and 26 °C in the freezing and thawing stages. In addition, daily minimum temperatures were less than 0 °C, but daily maximum temperatures were greater than °C. If we assume that soil starts to freeze when the temperature is <0 °C, there will essentially be a diurnal freeze/thaw cycle at 0·02 m depth. This was demonstrated by the significant diurnal range of 0·068 m^3 m^{-3} for unfrozen soil water content at 0–0·03 m depth in the freezing stage. However, unfrozen soil water at 0–0·03 m depth still had a low diurnal range of 0·02 m^3 m^{-3} in the thawing stage, which results from the low total soil water content (unfrozen water and ice). This low total soil water content is caused by two factors: (1) the surface frozen soil undergoes sublimation for approximately one month (the completely frozen stage), and (2) precipitation is very low in winter. A similar phenomenon can be found at a depth of 0·04 m; however, diurnal ranges of soil temperature and unfrozen soil water at 0·04 m depth were relatively lower than those at 0·02 m depth in the freezing and thawing stages, indicating a relatively weak diurnal freeze/thaw cycle. Furthermore, soil showed almost no diurnal freeze/thaw cycle at a depth of 0·1 m.

Observed diurnal variation of radiation components. Diurnal variations of downward short-wave radiation, upward short-wave radiation, and upward long-wave radiation were observed in all freeze/thaw stages, whereas diurnal variations of downward long-wave radiation were

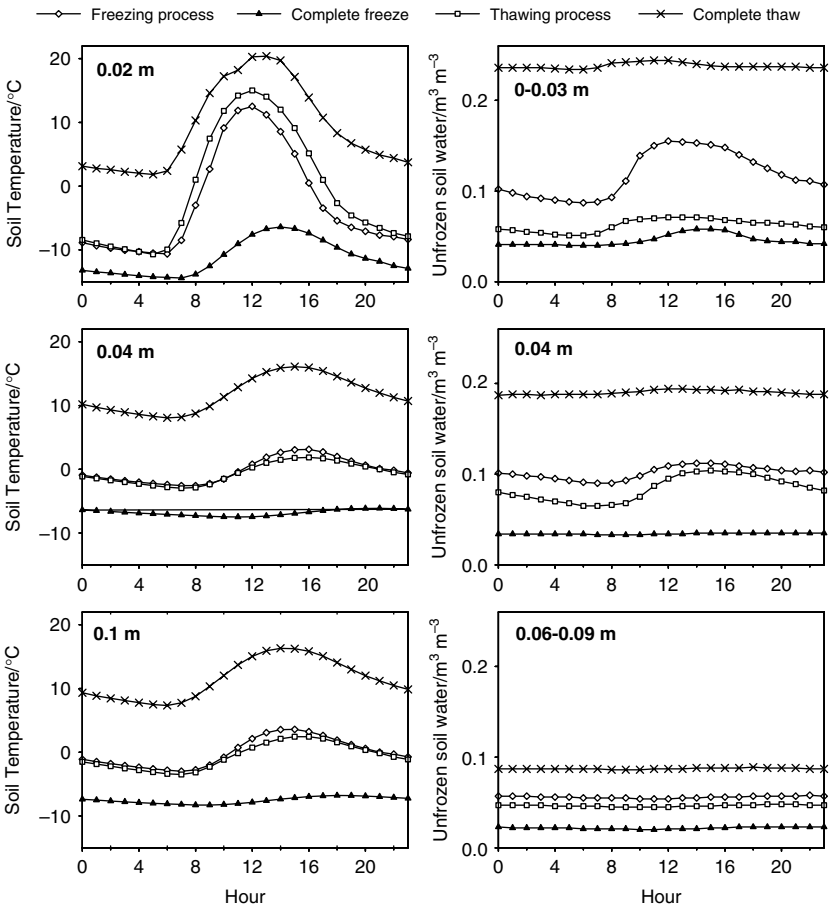

Figure 3. Diurnal variations of soil temperature and unfrozen water content at different depths averaged in the freezing, completely frozen, thawing, and completely thawed stages. Soil temperature and unfrozen water content are from the measurements

relatively weak (Figure 4). Downward short-wave radiation, upward long-wave radiation, and downward long-wave radiation were large in the completely thawed stage but weak in the completely frozen stage. In contrast, upward short-wave radiation was large in the completely frozen stage but weak in the completely thawed stage. The large upward short-wave radiation resulted from the large albedo of the snow-covered surface (0·68) in the completely frozen stage (Table III). Weak upward short-wave radiation resulted from the increase in the surface wetness and growth of the grass in the completely thawed stage. On average, the maximum downward short-wave radiation occurred at 11 : 00 and reached 642, 683, and 683 W m^{-2} in the freezing, thawing, and completely thawed stages, respectively. The maximum upward short-wave radiation also occurred at 11 : 00 and reached 152, 181, and 116 W m^{-2} in each of these three stages, respectively. In the completely frozen stage, however, the maximum downward and upward short-wave radiation occurred at 12 : 00, with a maximum downward value of 609 W m^{-2} and a maximum upward value of 415 W m^{-2}. The maximum downward long-wave radiation occurred at 12 : 00 and reached 237, 202, and 335 W m^{-2} in the freezing, completely frozen, and completely thawed stages respectively, but occurred at 13 : 00 and reached 256 W m^{-2} in the thawing stage. The maximum upward long-wave radiation in all stages occurred at 12 : 00 and reached levels of 387, 302, 405, and 442 W m^{-2} for the freezing, completely frozen, thawing, and completely thawed stages, respectively. The minimum upward long-wave radiation occurred at 5 : 00, 3 : 00, 5 : 00, and 4 : 00, and reached 260, 204, 260, 335 W m^{-2} during the freezing, completely frozen, thawing, and completely thawed stages, respectively. The data for the mean radiation components in different freeze/thaw stages are presented in Table III.

Diurnal variation of energy components. The sensible and latent heat fluxes were simulated results; net radiation was derived from measurements; and the soil heat flux was calculated by Equation (3). The diurnal variations of net radiation, latent heat flux, and soil heat flux were largest in the completely thawed stage and smallest in the completely frozen stage (Figure 4); however, the largest diurnal variation of sensible heat flux occurred in the thawing stage but not in the completely thawed stage. This may result from the primary allocation of solar radiation to latent heat of evaporation due to high levels of precipitation in the completely thawed stage. As the sun rose at about 6 : 00, the net radiation in all stages started to increase rapidly to extreme peaks of 335, 95, 349, and 461 W m^{-2} in the freezing, completely frozen, thawing, and completely thawed stages, respectively, until approximately 11 : 00, then decreased

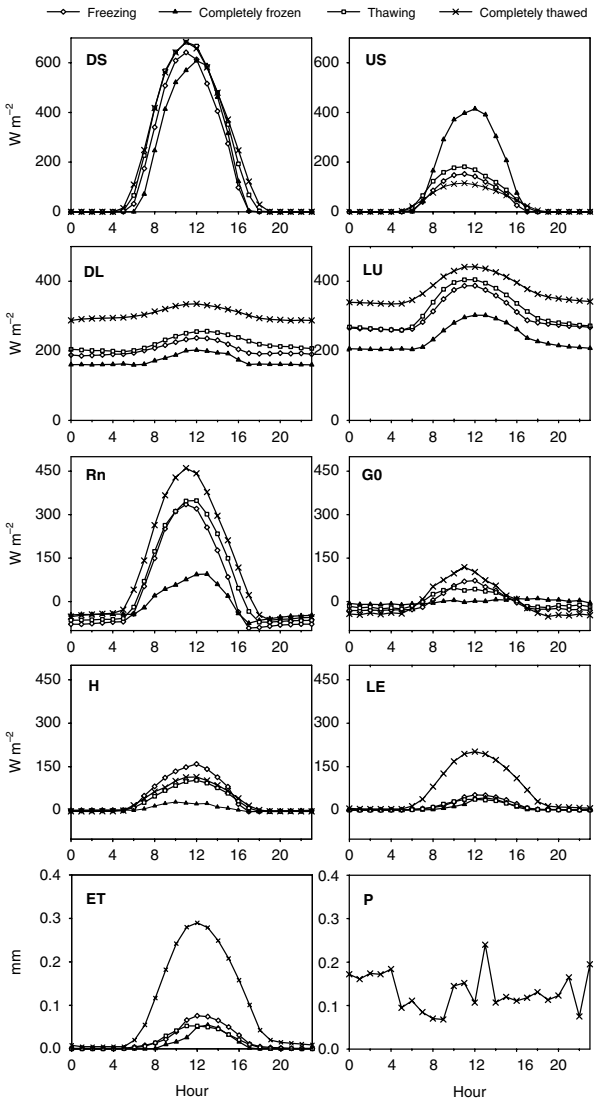

Figure 4. Diurnal variations of land surface heat and water exchange components averaged in the freezing, completely frozen, freezing, and completely thawed stages. DS refers to downward short-wave radiation, US refers to upward short-wave radiation, DL refers to downward long-wave radiation, UL refers to upward long-wave radiation, Rn refers to net radiation, H refers to sensible heat flux, LE refers to latent heat flux, G0 refers to soil surface heat flux, ET refers to evapotranspiration per hour, and P refers to precipitation per hour. Note that H, LE, and ET are the simulated results, G0 is calculated by Equation (3), and the other variables are from the measurements

quickly. The diurnal variation of net radiation in the complete frozen stage was distinctly weaker than that in the other stages, and this may have been caused by larger upward short-wave radiation resulting from dry ground and the large albedo of the snowpack in the complete frozen stage. Sensible heat flux in all stages started to increase at approximately 6 : 00, and reached extreme peak values of 159, 27, 103, and 114 W m^{-2} in the freezing, completely frozen, thawing, and completely thawed stages, respectively, at approximately 12 : 00. The diurnal variation of latent heat flux in the completely thawed stage was distinct from those in the other stages because of frequent precipitation. The Bowen ratios were 3·1, 0·7, 2·5, and 0·5 in the freezing, completely frozen, thawing, and completely thawed stages, respectively. This indicates that sensible heat flux was the main consumer of available energy at the surface during the freezing and thawing stages. Soil heat flux was positive from 7 : 00 to 14 : 00, but negative at other times of the day.

Simulated diurnal variation of evapotranspiration. Evapotranspiration had obvious diurnal variation in all freeze/thaw stages (Figure 4). Its diurnal variation was relatively weak in the completely frozen stage, but distinctly significant in the completely thawed stage due to much stronger diurnal variation of available energy (i.e. net radiation) in this stage. Evapotranspiration started to increase at about 6 : 00 and reached a peak with values of 0·09, 0·06, 0·10, and 0·30 mm/h at about 11 : 00 in each of the freezing, completely frozen, thawing, and completely thawed stages. It then deceased quickly. This pattern of variation demonstrates the dependence of evapotranspiration on solar radiation.

Cumulative evapotranspiration was larger than precipitation during the freezing and thawing stages (Table III), and it is equivalent to precipitation in the completely frozen stage. The ratio of evapotranspiration to precipitation reached 73% in the completely thawed stage. Similar results can be found in previous works, such as a ratio of 73·2% on the south sides of the Tanggula Mountains based on observational data from GAME-Tibet (Yang *et al*., 2007b) and approximately 70% near Naqu, south of the Tanggula Mountains, based on numerical simulation (Numaguti, 1998). These results show that local evapotranspiration has a considerable contribution to the Tibetan summer precipitation.

Cumulative evapotranspiration (40 mm) was obviously larger than precipitation in the thawing stage. This may result from very high unfrozen soil water when

Table III. Mean radiation and energy components (W m^{-2}) as well as cumulative evapotranspiration (mm) and precipitation (mm) in different freeze/thaw stages at site BJ for the period from August 2002 to August 2003. DS refers to downward short-wave radiation, US refers to upward short-wave radiation, DL refers to downward long-wave radiation, UL refers to upward long-wave radiation, Rn refers to net radiation, H refers to sensible heat flux, LE refers to latent heat flux, β refers to Bowen ratio, and G0 refers to soil heat flux, ET refers to cumulative evapotranspiration, and P refers to cumulative precipitation. Note that H, LE, and ET are the simulated results, G0 is calculated by Equation (3), and the other variables are from the measurements

	DS	US	Albedo	DL	UL	Rn	H	LE	β	G0	ET	P	ET/P
Freezing	176	42	0·24	203	302	35	43	14	3·1	−3·4	42	11	3·80
Completely frozen	163	111	0·68	171	237	−13	6	9	0·7	−0·7	6	6	1·00
Thawing	206	55	0·27	221	314	59	28	11	2·5	0·7	40	14	2·90
Completely thawed	215	37	0·17	305	375	107	33	67	0·5	1·6	330	453	0·73

the ground has just thawed in this stage. Such high unfrozen soil water results from the frozen ground storing water from precipitation for almost six months during the completely thawed stage in the prior year. At the same time, due to the lower albedo of the thawed soil, the increased ability to absorb solar radiation at the soil surface would make the ground temperature rise, favouring the evaporation of unfrozen soil water (Yang *et al*., 2003). This process may also occur during the freezing stage because the surface soil is still in a thawed state—at lower albedo—during the daytime for this stage, but high unfrozen soil water in the freezing stage may derive from deep percolated precipitation during the completely thawed stage.

Correlation between heat fluxes and soil temperature and unfrozen soil water

In this section, the sensible and latent heat fluxes were taken from the simulated data; however, soil temperature, unfrozen soil water, and weather data were taken from the measurements. To quantify the influences of the diurnal freeze/thaw cycles on land-atmosphere interactions, we investigated the relationships between surface heat fluxes and the ground temperature, air temperature, unfrozen soil water, and air humidity during the four freeze/thaw stages (Table IV). Except for the completely frozen stage, latent heat flux had the best correlations with the ground temperature, and also good correlations with air temperature at 1 m above the surface in the other freeze/thaw stages. Sensible heat flux also had the best correlations with the ground temperature and had good correlations with air temperature at 1 m above the surface in all freeze/thaw stages. Both sensible and latent heat fluxes showed negative correlations with air humidity at 1 m above the surface. This was especially evident in the completely thawed stage because air humidity was relatively large due to frequent precipitation in this stage.

As seen in Table IV, the correlation coefficients between sensible heat flux and unfrozen soil water are quite small in all soil freeze/thaw stages. It was also noted that latent heat flux showed almost no correlation with unfrozen soil water at a depth of 0·04 m in the completely frozen and thawed stages. Instead, rather low or even no unfrozen soil water content resulted in almost zero correlation with latent heat flux in the completely frozen stage. In contrast, sufficient unfrozen soil water content during the daytime and at night made latent heat flux more dependent on air temperature and soil temperature in the completely thawed stage. However, latent heat flux exhibited distinctly better correlations with unfrozen soil water in the freezing stage than those in the completely frozen and thawed stages. Moreover, such correlations decreased as soil depth increased. This implies that the near-surface unfrozen soil water change resulting from the diurnal freeze/thaw cycle had a significant influence on latent heat flux. Such a conclusion is also applicable for the thawing stage, although the correlation coefficients between latent heat flux and unfrozen soil water in the thawing stage were smaller than those in the freezing stage. Thus, the impact of near-surface unfrozen soil water change on latent heat flux was larger in the freezing stage than in the thawing stage.

Analysis of surface energy budget

The surface energy budget is the most fundamental factor influencing biosphere-atmosphere feedbacks, and its diurnal variations are sensitive in climate simulations. Missing energy could, therefore, be a significant source of error in existing atmospheric models. Recent recognitions of surface energy closure failure have resulted in rigorous investigations and convictive interpretations (e.g. Gao *et al*., 2009a; Wever *et al*., 2002; McCaughey *et al*., 1997; Stannard *et al*., 1994). To investigate the surface energy budget during different soil freeze/thaw conditions, we simulated sensible and latent heat fluxes from August 2002 to August 2003 using the SHAW model. The model can reasonably simulate surface heat fluxes in the freezing/thawing and the completely thawed stage, which was validated in an earlier section. The net radiation used here was still derived from observations, and the soil heat flux used here was calculated by Equation (3). The closure ratio (CR) is defined as the ratio of the sum of sensible and latent heat fluxes to the total available energy sum of net radiation and soil heat fluxes. Theoretically, the CR should be equal or almost equal to 1·0 for a level and homogeneous observation field having

Table IV. Correlation coefficients between hourly land surface heat fluxes and the ground temperature (Ts), air temperature (Ta), unfrozen soil water (usw), and air humidity (qa) during the four freeze/thaw stages. H and LE refer to sensible and latent heat flux*. H and LE are the simulated results and the other variables are from the measurements

		$Ts_{0\ m}$	$Ta_{1\ m}$	$usw_{0\sim0.03\ m}$	$usw_{0.04\ m}$	$usw_{0.06\sim0.09\ m}$	$qa_{1\ m}$
Freezing	LE	0·69	0·58	0·53	0·40	0·36	−0·30
	H	0·51	0·53	0·19	0·05[a]	0·01[a]	−0·5
Completely frozen	LE	0·27	0·50		−0·08[a]		−0·40
	H	0·24	0·23		0·01[a]		−0·28
Thawing	LE	0·61	0·54	0·45	0·39	0·36	−0·24
	H	0·63	0·50	0·13	0·12	0·04[a]	−0·45
Completely thawed	LE	0·86	0·74		0·07[a]		−0·76
	H	0·66	0·51		0·08[a]		−0·59

[a] Correlation coefficients do not exceed the 99% confidence level

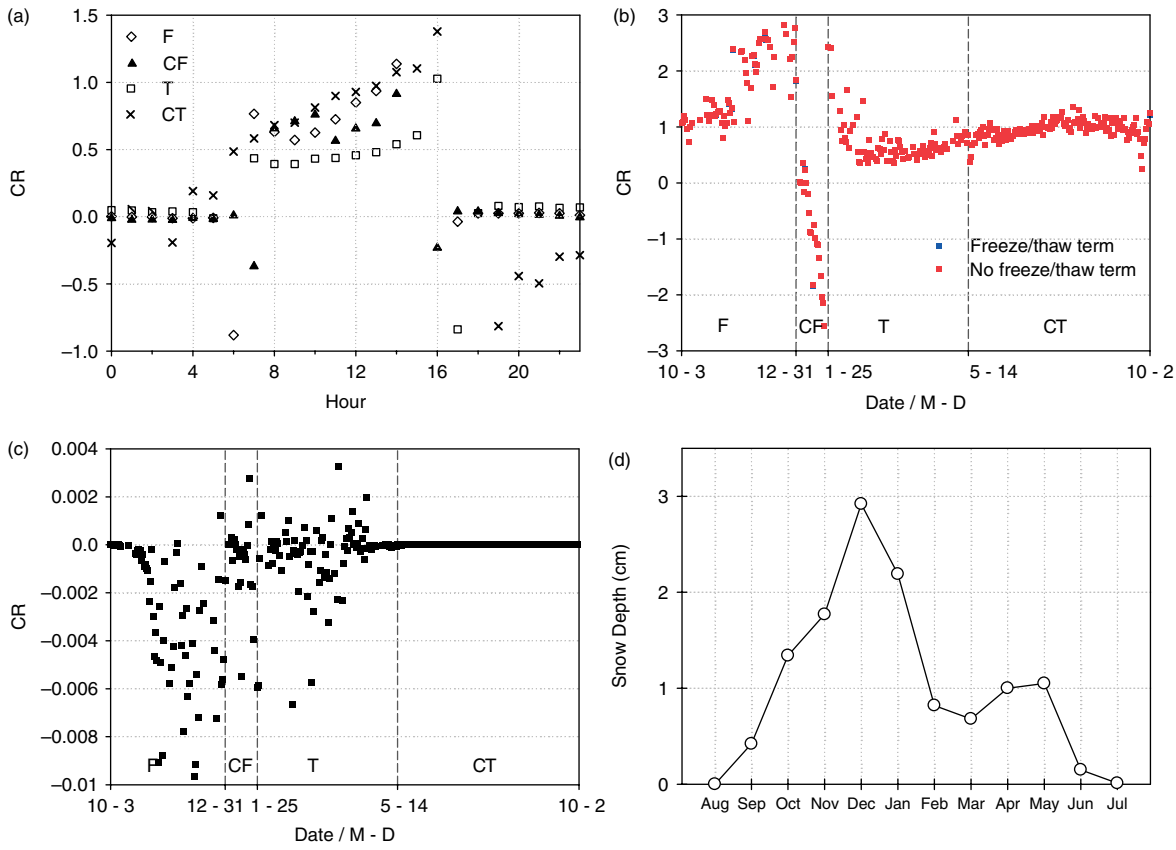

Figure 5. Diurnal variations of closure ratio (CR) averaged in different freeze/thaw stages (a), annual variation of daily average CR (b), deviation between CR values with freeze/thaw term and without freeze/thaw term (c), and monthly (August–July) snow depths averaged for the 34 years from 1966 to 1999 at Naqu meteorological station (d). F refers to the freezing stage, CF refers to the completely frozen stage, T refers to the thawing stage, and CT refers to the completely thawed stage. CR is calculated by the observed net radiation, the simulated sensible and latent heat fluxes, and the calculated soil heat flux

a sufficient number of fetches or footprint. In this study, days with snowfall were eliminated due to the large influence of snowfalls on the surface energy balance when calculating the CR (Yao *et al.*, 2008).

Mean CR displayed similar diurnal variation patterns in the four freeze/thaw stages (Figure 5-(a)). From about 8 : 00 to about 14 : 00, CR ranged from 0·40 to 1·10 in all four freeze/thaw stages, but CR was close to zero from about 17 : 00 to about 5 : 00 in the next morning. Thus, the degree of energy closure was better during the daytime than at night, which agrees with other critically important results from the International Network of Eddy Covariance Site (FLUXNET) and ChinaFLUX (Wilson *et al.*, 2002; Li *et al.*, 2005). Daily CR fluctuated between 0·30 and 1·30 in the completely thawed stage, with an average of 0·95 (Figure 5-(b)). Mean daily CR values were 1·60 and 0·73 in the freezing and thawing stages, respectively. Unexpectedly, diurnal average CR was negative in the completely frozen stage, with an average value of −0·72.

The mean daily CR value was greater than 1 during the freezing process but less than 1 during the thawing process stage. Generally, CR >1 results from the overestimated soil heat flux due to the heat released by the freezing process of the frozen soil water during the freezing stage. In contrast, CR <1 results from the underestimated soil heat flux because of the heat absorbed by the melting process of the frozen soil water during the thawing stage. To examine the extent to which the soil freeze/thaw processes affect the energy balance closure, we compared the results from the Equation (3) with the freeze/thaw term and without freeze/thaw term (Figure 5(b,c)). The inclusion of freeze/thaw term produced a reasonably lower mean daily CR value 1·59 compared to 1·60 of the no-freeze/thaw term during the freezing stage and almost unchanged mean daily CR value during the thawing stage. However, the deviations between the CR values were small, indicating a weak impact of soil freeze/thaw process on the energy balance closure.

Exploring the reasons for energy balance closure failure in detail is beyond the scope of this paper; however, previous studies have shown that the heat stored within the vegetation mass could affect the energy balance closure (Blanken *et al.*, 1997; Arain *et al.*, 2003; Wu *et al.*, 2007). Blanken *et al.* (1997) found that the energy balance components could be largely influenced by the leaf area change of the species overstory and understory in a boreal aspen forest. At the BJ site, vegetation cover is consists of short grass, with LAI <0·2 during the weak growth stage from October to April, as well as a canopy height <0·05 m and LAI <0·5 during the peak growth stage from late May to mid-September. Compared to a maximum forest leaf area index of 5·6 from Blanken *et al.* (1997), the LAI of site BJ is distinctly

small. Thus, it seems that vegetation is still not a leading error source for energy balance closure at this site.

Yao *et al*. (2008) demonstrated that the large albedo of the snowpack resulted in the decrease in net radiation and the associated low CR. Moreover, a significant error source for CR may be in the melt of the snowpack and in the heat stored due to the thermal mass of the snowpack. At the Naqu meteorological station near site BJ (Figure 1), on average, snow is present from September to the following June (Figure 5(d)). Monthly snow depth averaged for 1966–1999 ranged from 0·15 to 2·92 cm. Assuming that precipitation is snowfall when air temperature $<0\,^{\circ}$C, monthly mean snowfall of 4·3 mm would occur from about October 2002 to about May 2003. Thus, thermal storage and melting of the snowpack may be a significant source of error for energy balance closure. Other sources not discussed here may also contribute to the energy balance closure failure. Careful evaluation of heat storage is important to obtaining surface energy balance closure (Lamaud *et al*., 2001; Jacobs *et al*., 2008).

CONCLUDING REMARKS

Our research shows that significant diurnal variation exists in the mean radiation and energy components, evapotranspiration, soil temperature, and unfrozen soil water at a depth of 0·02 m in all four freeze/thaw stages. Near-surface soil experiences diurnal freeze/thaw cycles during the freezing and thawing stages. The diurnal freeze/thaw cycle of near-surface soil has a significant impact on the surface heat flux change, and this impact is more evident in the freezing stage than in the thawing stage. The ground energy imbalance problem is encountered in all four soil freeze/thaw stages. Our analysis substantiates that the freeze/thaw processes in near-surface soil have impact on the energy balance closure failure, but such impact is weak at this site. The energy imbalance problem may relate to thermal storage and melting of the snowpack. These results provide some insights into the impacts of soil freezing/thawing processes on energy and water exchanges between land surface and atmosphere on the central Tibetan Plateau.

Although the SHAW model is validated to be applicable for surface heat and water transfer estimation on the Tibetan Plateau, the simulated sensible and latent heat fluxes and evapotranspiration may still cause bias for the surface energy closure budget to some extent. Thus, long-term observations of the parameters (e.g. surface heat fluxes, soil heat flux) are required in the future to obtain a more accurate examination of the surface energy budget closure on a yearly scale over the Tibetan Plateau. In addition, our present work is based on only one observational site, and future work needs to scale up to the regional scale, or even the whole Plateau region, by merging the regional measurements, atmospheric models, remote sensing, and data assimilation methodologies.

ACKNOWLEDGMENTS

This research was jointly supported by the National Basic Research Program of China (973 Program) under Grant 2009CB421406, the Chinese Academy of Sciences under Grants KZCX2-YW-Q1-02 and KZCX2-YW-Q11-05, the Norwegian Research Council project "East-Asia DecCen.", the Natural Science Foundation of China (41075007), the One Hundred Talent Program of the Chinese Academy of Sciences (29O827B11), the Key International Cooperation Project of NSFC (40810059006), and National Key Basic Research program of China (2010CB951404). Opinions, findings, conclusions, and recommendations expressed in this paper are those of the authors and do not necessarily reflect the views of the National Science Foundation. We are indebted to three reviewers for helpful comments and criticisms of the initial draft of this paper.

REFERENCES

Arain MA, Black TA, Barr AG, Griffis TJ, Morgenstern K, Nesic Z. 2003. Year-round observations of the energy and water vapour fluxes above a boreal black spruce forest. *Hydrological Processes* **17**: 3581–3600.

Barnett TP, Dumenil L, Schlese U, Roeckner E, Latif M. 1989. The effect of Eurasian snow cover on regional and global climate variations. *Journal of Atmospheric Sciences* **46**: 661–685.

Blanken PD, Black TA, Yang PC, Neumann HH, Nesic Z, Staebler R, Hartog G, Novak MD, Lee X. 1997. Energy balance and canopy conductance of a boreal aspen forest: Partitioning overstory and understory components. *Journal of Geophysical Research* **102**(D24): 28915–28927.

Choi T, Hong J, Kim J, Lee H, Asanuma J, Ishikawa H, Tsukamoto O, Gao Z, Ma Y, Ueno K, Wang J, Koike T, Yasunari T. 2004. Turbulent exchange of heat, water vapor, and momentum over a Tibetan prairie by eddy covariance and flux variance measurements. *Journal of Geophysical Research* **109**: D21106, DOI:10.1029/2004JD004767.

Flerchinger GN, Saxton KE. 1989. Simultaneous heat and water model of a freezing snow-residue-soil system, I, theory and development. *Transactions of the Asae* **32**: 567–571.

Flohn H. 1957. Large-scale aspects of the "summer monsoon" in south and East Asia. *Journal Meteorology Society of Japan*, 75th anniv., vol., 180–186.

Gao Z, Chae N, Kim J, Hong J, Choi T, Lee H. 2004. Modeling of surface energy partitioning, surface temperature, and soil wetness in the Tibetan prairie using the Simple Biosphere Model 2 (SiB2). *Journal of Geophysical Research* **109**: D06102, DOI:10.1029/2003JD004089.

Gao Z, Lenschow DH, He Z, Zhou M, Wang L, Wang Y, He J, Shi J. 2009a. Seasonal and diurnal variations in moisture, heat and CO_2 fluxes over a typical steppe prairie in Inner Mongolia, China. *Hydrology and Earth System Sciences Discussions* **6**: 1939–1972.

Gao Z, Wang J, Ma Y, Kim J, Choi T, Lee H, Asanuma J, Su Z. 2000a. Study of roughness lengths and drag coefficients over Nansha Sea Region, Gobi, desert, oasis and Tibetan Plateau. *Physics and Chemistry of the Earth (B)* **25**: 141–145.

Gao Z, Wang J, Ma Y, Kim J, Choi T, Lee H, Asanuma J, Su Z. 2000b. Calculation of near-surface layer turbulent transport and analysis of surface thermal equilibrium features in Naqu of Tibet. *Physics and Chemistry of the Earth (B)* **25**: 135–139.

Guo DL, Yang MX, Li M, Qu P. 2009a. Analysis on simulation of characteristic of land surface energy flux in seasonal frozen soil region of central Tibetan Plateau. *Plateau Meteorology (in Chinese)* **28**: 978–987.

Guo DL, Yang MX, Qu P, Wan GN, Wang XJ. 2009b. Studies of the energy and water cycle processes: review and discussion. *Journal of Glaciology and Geocryology (in Chinese)* **31**: 1116–1126.

Guo DL, Yang MX. 2010. Simulation of soil temperature and moisture in seasonally frozen ground of central Tibetan Plateau by SHAW model. *Plateau Meteorology (in Chinese)* **29**: 1369–1377.

Guo DL, Yang MX, Wang HJ. 2011. Sensible and latent heat flux response to diurnal variation in soil surface temperature and moisture

under different freeze/thaw soil conditions in the seasonal frozen soil region of the central Tibetan Plateau. *Environmental Earth Sciences*, in press, DOI: 10.1007/s12665-010-0672-6.

Jacobs AFG, Heusinkveld BG, Holtslag AAM. 2008. Towards Closing the Surface Energy Budget of a Mid-latitude Grassland. *Boundary-Layer Meteorology* **126**: 125–136.

Kim J, Choi T, Lee H, Hong J, Kim J, Wang J, Gao Z, Yan Y, Ma Y, Asanuma J, Koike T, Yasunari T. 2000a. Energy partitioning and its imbalance over a prairie site in central Tibetan plateau during GAPE-IOP. 1998, *Eos Trans. AGU*, 2000, **81**(22): 5.

Kim J, Hong J, Gao Z, Choi T. 2000b. Can we close the surface energy budget in the Tibetan Plateau?. Paper presented at Second Session of International Workshop on TIPEX- GAME/Tibet, Joint Coord. Comm., TIPEX-GAME/Tibet, Kunming, China.

Lamaud E, Ogee J, Brunet Y, Berbigier P. 2001. Validation of eddy flux measurements above the understorey of a pine forest. *Agricultural and Forest Meteorology* **106**: 187–203.

Li C, Yanai M. 1996. The onset and interannual variability of the Asian summer monsoon in relation to land-sea thermal constrast. *Journal of Climate* **9**: 358–375.

Li S, Nan Z, Zhao L. 2002. Impact of soil freezing and thawing process on thermal exchange between atmosphere and ground surface. *Journal of Glaciology and Geocryology* (in Chinese) **24**(5): 506–511.

Li Z, Yu G, Wen X, Zhang L, Ren C, Fu Y. 2005. Energy balance closure at ChinaFLUX sites. *Science in China (Series D)* **48**(1): 51–62.

Liu X, Kutzbach JE, Liu Z, An Z, Li L. 2003. The Tibetan Plateau as amplifier of orbital-scale variability of the East Asian monsoon. *Geophysical Research Letter* **30**: 1839, DOI:10.1029/2003GL017510.

Luo S, Lv S, Zhang Y, Hu Z, Ma Y, Li S, Shang L. 2008. Simulation analysis on land surface process of BJ site of central Tibetan Plateau Using CoLM. *Plateau Meteorology* (in Chinese) **27**(2): 259–271.

Ma W, Ma Y. 2006. The annual variations on land surface energy in the northern Tibetan Plateau. *Environmental Geology* **50**(5): DOI:10.1007/s00254-006-0238-9.

Ma Y, Fan S, Ishikawa H, Tsukamoto O, Yao T, Koike T, Zuo H, Hu Z, Su Z. 2004. Diurnal and inter-monthly variation of land surface heat fluxes over the central Tibetan Plateau area. *Theoretical and Applied Climatology* **80**: 259–273.

Ma Y, Tsukamoto O, Wang J, Ishikawa H, Tamagawa I. 2002. Analysis of aerodynamic and thermodynamic parameters on the grassy marshland surface of Tibetan Plateau. *Progress in Nature Science* **12**: 36–40.

Ma Y, Yao T, Wang J. 2006. Experimental study of energy and water cycle in Tibetan Plateau-the progress introduction on the study of GAME/Tibet and CAMP/Tibet. *Plateau Meteorology* (in Chinese) **25**(2): 344–351.

McCaughey JH, Lafleur PM, Joiner DW, Bartlett PA, Costello AM, Jelinski DE, Ryan MG. 1997. Magnitudes and seasonal patterns of energy, water, and carbon exchanges at a boreal young jack pine forest in the BOREAS northern study area. *Journal of Geophysical Research* **102**(D24): 28997–29007.

Numaguti A. 1998. Origin and recycling processes of precipitating water over the Eurasian continent: Experiments using an atmospheric general circulation model. *Journal of Geophysical Research* **104**: 1957–1972.

Oleson KW, Dai Y, Bonan G, Bosilavich M, Dickinson T, Dirmeyer P, Hoffman F, Houser P, Levis S, Niu G-Y, Thornton P, Vertenstein M, Yang Z-L, Zeng X. 2004. Technical description of the community land model (CLM). NCA technical note, NCAR/TN-461+STR.

Sellers PJ, Randall DA, Collatz GJ, Berry JA, Field CB, Dazlich DA, Zhang C, Collelo G D, Bounoua L. 1996a. A revised land surface parameterization (SiB2) for atmospheric GCMs. Part I: Model formulation. *Journal of Climate* **9**: 676–705.

Sellers PJ, Los SO, Tucker CJ, Justice CO, Dazlich DA., Collatz GJ, Randall DA. 1996b. A revised land surface parameterization (SiB2) for atmospheric GCMs. part II: The generation of global fields of terrestrial biophysical parameters from satellite data. *Journal of Climate* **9**: 706–737.

Stannard DI, Blanford JH, Kustas WP, Nichols WD, Amer SA, Schmugge TJ, Weltz MA. 1994. Interpretation of surface flux measurements in heterogeneous terrain during the Monsoon'90 experiment. *Water Resources Research* **30**(5): 1227–1239.

Su Z, Zhang T. 2006. Energy and Water Cycle over the Tibetan Plateau Surface energy balance and turbulent heat fluxes. *Advance in Earth Science* **21**(12): 1224–1236.

Tanaka K, Ishikawa H, Hayashi H, Tamagama I, Ma Y. 2001. Surface energy budget at Amdo on the Tibetan Plateau using GAME/Tibet IOP 98 data. *Journal of the Meteorological Society of Japan* **79**(1B): 505–517.

Tanaka K, Tamagawa I, Ishikawa H, Ma Y, Hu Z. 2003. Surface energy budget and closure of the eastern Tibetan Plateau during the GAME-Tibet IOP 1998. *Journal of Hydrology* **283**: 169–183.

Tsukamoto O, Ishikawa H, Miyazaki S, Kim J, Ma Y, Hu Z. 2001. Diurnal variations of surface fluxes and boundary layer over Tibetan Plateau. Proceedings of the International Workshop on GAME-AAN/Radiation, Phuket, Thailand 7–9 March, 2001 (Bulletin of the Terrestrial Environment Research Center, University of Tsukuba, No. 1 Supplement), pp. 36–39.

Vernekar AD, Zhou J, Shukla J. 1995. The effect of Eurasian snow cover on the Indian monsoon. *Journal of Climate* **8**: 248–266.

Wang C, Dong W, Wei Z. 2003. Study on relationship between the frozen-thaw process in Qinghai-Xizang Plateau and circulation in East-Asia. *Chinese Journal of Geophysics* **46**(3): 309–316.

Webster PJ. 1987. In *Monsoons*, Fein JS, Stephens PL. (eds). Wiley: New York; pp. 3–32.

Wever LA, Flanagan LB, Carlson PJ. 2002. Seasonal and interannual variation in evapotranspiration, energy balance, and surface conductance in northern temperate grassland. *Agricultural and Forest Meteorology* **112**: 31–49.

Wilson K, Goldstein A, Falge E, Aubinet M, Baldocchi D, Beibigier P, Bernhofer C, Ceulemans R, Dolman H, Field C, Grelle A, Ibrom A, Law BE, Kowalski A, Meyers T, Moncrieff J, Monson R, Oechel W, Tenhunen J, Valentini R, Verma S. 2002. Energy balance closure at FLUXNET sites. *Agricultural and Forest Meteorology* **113**: 223–243.

Wu J, Guan D, Han S, Shi T, Jin C, Pei T, Yu G. 2007. Energy budget above a temperature mixed forest in northeastern China. *Hydrological Processes* **21**: 2425–2434.

Xu J, Haginaya S. 2001. An estimation of heat and water balances in the Tibetan Plateau. *Journal of the Meteorological Society of Japan* **79**(1B): 485–504.

Yanai M, Li CY, Song Z. 1992. Seasonal heating of the Tibetan Plateau and its effects on the evolution of Asian summer monsoon. *Journal of Meteorology Society of Japan* **70**: 319–351.

Yang K, Koike T, Ishikawa H, Ma Y. 2003. Analysis of the surface energy budget at a site of GAME/Tibet using a single-source model. *Journal of Meteorology Society of Japan* **106**: 245–262.

Yang K, Wang J. 2008. A temperature prediction-correction method for estimating surface soil heat flux from soil temperature and moisture data. *Science in China (Series D)* **51**: 721–729.

Yang M, Yao T, Gou X. 2003. The soil moisture distribution, thawing-freezing processes and their effects on the seasonal transition on the Qinghai-Xizang(Tibetan) plateau. *Journal of Asian Earth Sciences* **21**: 457–465.

Yang M, Yao T, Gou X, Nozomu H, Yuki FH, Hao L, Levia DF. 2007a. Diurnal freeze/thaw cycles of the ground surface on the Tibetan Plateau. *Chinese Science Bulletin* **52**(1): 136–139.

Yang M, Yao T, Gou X, Tang H. 2007b. Water recycling between the land surface and atmosphere on the Northern Tibetan Plateau—A case study at flat observation sites. *Arctic, Antarctic, and Alpine Research* **39**(4): 1–5.

Yao J, Zhao L, Ding Y, Gu L, Jiao K, Qiao Y, Wang Y. 2008. The surface energy budget and evapotranspiration in the Tanggula region on the Tibetan Plateau. *Cold Regions Science and Technology* **52**: 326–340.

Ye D, Gao Y. 1979. *Meteorology of the Tibetan Plateau*. Science press: Beijing; 30–55.

Yeh TC, Dao SY, Li MT. 1957. *The abrupt change of circulation over the North Hemisphere during June and October, The Atmosphere and the Sea in Motion, Rossby Memorial Volume*, pp. 249–267, Rockefeller Inst. Press: Albany, NY.

